

This is a repository copy of *A new diagnostic for tropospheric ozone production*.

White Rose Research Online URL for this paper:

<https://eprints.whiterose.ac.uk/117197/>

Version: Submitted Version

Article:

Edwards, Peter M. orcid.org/0000-0002-1076-6793 and Evans, Mathew J. orcid.org/0000-0003-4775-032X (2017) A new diagnostic for tropospheric ozone production. *Atmospheric Chemistry and Physics*. pp. 13669-13680. ISSN 1680-7324

<https://doi.org/10.5194/acp-17-13669-2017>

Reuse

This article is distributed under the terms of the Creative Commons Attribution (CC BY) licence. This licence allows you to distribute, remix, tweak, and build upon the work, even commercially, as long as you credit the authors for the original work. More information and the full terms of the licence here:

<https://creativecommons.org/licenses/>

Takedown

If you consider content in White Rose Research Online to be in breach of UK law, please notify us by emailing eprints@whiterose.ac.uk including the URL of the record and the reason for the withdrawal request.



1 **A new diagnostic for tropospheric ozone production**

2 Peter M. Edwards^{1*} & Mathew J. Evans^{1,2}

3 ¹ Wolfson Atmospheric Chemistry Laboratories, Department of Chemistry, University of York,
4 Heslington, York, YO10 5DD, UK

5 ² National Centre for Atmospheric Science, Department of Chemistry, University of York, Heslington,
6 York, YO10 5DD, UK

7 *pete.edwards@york.ac.uk

8 **Abstract**

9 Tropospheric ozone is important for the Earth's climate and air quality. It is produced
10 during the oxidation of organics in the presence of nitrogen oxides. Due to the range
11 of organic species emitted and the chain like nature of their oxidation, this chemistry
12 is complex and understanding the role of different processes (emission, deposition,
13 chemistry) is difficult. We demonstrate a new methodology for diagnosing ozone
14 production based on the processing of bonds contained within emitted molecules, the
15 fate of which is determined by the conservation of spin of the bonding electrons.
16 Using this methodology to diagnose ozone production in the GEOS-Chem chemical
17 transport model, we demonstrate its advantages over the standard diagnostic. We
18 show that the number of bonds emitted, their chemistry and lifetime, and feedbacks on
19 OH are all important in determining the ozone production within the model and its
20 sensitivity to changes. This insight may allow future model-model comparisons to
21 better identify the root causes of model differences.

22 **1. Introduction**

23 The chemistry of the troposphere is one of oxidation [*Levy, 1973; Kroll et al., 2011*].
24 Organic compounds together with nitrogen and sulfur containing molecules are
25 emitted into the troposphere where they are oxidised into compounds which can either
26 be: absorbed by the biosphere; are involatile enough to form aerosols; can deposit to
27 the surface; or be taken up by clouds and rained out. The oxidation of these
28 compounds is significantly slower than might be expected based on the atmospheric
29 composition of 20% molecular oxygen (O₂). The inefficiency of ground state O₂ as an
30 atmospheric oxidant is due to its electronic structure. With two unpaired electrons it
31 is a spin-triplet (total spin quantum number S=1, giving a term symbol of ³Σ_g⁻). In



32 contrast, virtually all trace chemicals emitted into the atmosphere contain only paired
33 electrons and are thus spin-singlets ($S=0$). From a simplistic perspective (i.e. ignoring
34 nuclear spin interactions, inter-system crossings, nuclear dipole effects etc.) the spin
35 selection rule, $\Delta S=0$, means that the reaction of ground state O_2 with most emitted
36 compounds is effectively spin forbidden. Electronically excited O_2 ($^1\Delta_g$ or $^1\Sigma_g^+$) is a
37 spin singlet and is more reactive in the atmosphere but low concentrations limit its
38 role [Larson and Marley, 1999]. Instead, atmospheric oxidation proceeds
39 predominantly via reactions with spin-doublet oxygen-derived species ($S=1/2$), notably
40 the hydroxyl (OH) and peroxy radicals ($RO_2 = HO_2, CH_3O_2, C_2H_5O_2$, etc.), or spin-
41 singlet species (e.g. ozone (O_3)).

42 One of the few spin-triplet species in the atmosphere other than O_2 is the ground state
43 of atomic oxygen ($O(^3P)$), which readily undergoes a spin allowed reaction with O_2 to
44 produce the spin-singlet O_3 molecule. This spin allowed reaction is responsible for the
45 creation of O_3 in both the stratosphere, where it forms the protective O_3 layer, and the
46 troposphere. The ability of O_3 to oxidise other spin-singlet species makes it a powerful
47 oxidant, and it is thus considered a pollutant with negative health effects. Sources of
48 $O(^3P)$ within the troposphere are limited because solar photons at sufficiently short
49 wavelengths to directly photolyse O_2 to $O(^3P)$ are essentially unavailable.

50 Aside from the photolysis of O_3 itself, the only other significant source of
51 tropospheric $O(^3P)$ is the photolysis of nitrogen dioxide (NO_2) [Crutzen, 1971].
52 Nitrogen oxides are emitted into the troposphere as nitrogen oxide (NO), which can be
53 oxidised to NO_2 by O_3 and other oxidants. A large thermodynamic energy barrier
54 prevents oxidation of NO to NO_2 by the OH radical [Nguyen *et al.*, 1998], and
55 therefore NO oxidation occurs through reaction with either O_3 or RO_2 . In terms of O_3
56 production, the oxidation of NO by O_3 forms a null cycle. Thus only the reaction of
57 NO with RO_2 leads to a net production of O_3 .

58 Exploring the distribution, source and sinks of tropospheric O_3 is a central theme of
59 atmospheric science. Chemical transport models (online and offline) are essential
60 tools enabling this understanding but their validity needs to be continually assessed.
61 Model-model comparison exercises are commonly performed to assess performance,
62 and comparisons of modelled O_3 budgets traditionally form part of this assessment
63 [Stevenson *et al.*, 2006; Wu *et al.*, 2007; Wild, 2007; Young *et al.*, 2013]. Ozone
64 production is diagnosed from the flux of NO to NO_2 via reaction with each of the



65 speciated RO₂ in the model's chemical schemes. This approach provides information
66 on the relative importance of the different RO₂ in the fast NO + RO₂ reactions within
67 the model, but gives very little detail on how the longer time scale model processes
68 (emissions, chemistry, deposition) influence O₃ production. Thus exploring the
69 reasons that models differ in their O₃ production is difficult and progress has been
70 slow.

71 A new diagnostic framework that links large scale model drivers such as emission,
72 chemistry, and deposition to O₃ production would allow an improved assessment of
73 why model ozone budgets differ. We attempt to provide such a framework here.

74 **2. A new diagnostic framework.**

75 The rate of production of tropospheric O₃ is limited by the rate of oxidation of NO to
76 NO₂, which is in turn limited by the rate of production of peroxy radicals (RO₂).
77 Peroxy radicals form through association reactions of hydrogen (H) atoms or alkyl
78 radicals (both spin-doublets, S=½) with O₂, forming a highly reactive spin-doublet
79 radical on an oxygen atom. This spin allowed reaction converts spin-triplet O₂ that
80 cannot react with spin-singlet pollutants into a spin-doublet O₂ containing species that
81 can. As such the formation of RO₂ is central to the atmosphere's oxidation capacity,
82 and its production is limited by the rate of production of H atoms or alkyl radicals.
83 Thus the maximum potential rate of tropospheric O₃ production is equal to the rate at
84 which H atoms and alkyl radicals are produced.

85 Hydrogen atoms and alkyl radicals are predominantly produced via the spin allowed
86 breaking of the spin-pairing between the two electrons in a C or H containing covalent
87 bond (S=0), such as those in hydrocarbons. These spin-pairings can be broken in the
88 atmosphere either chemically or photolytically, with the products necessarily
89 conserving spin. The breaking of a covalent bond by a photon (s=1) can result in two
90 products with S=½ or two products with S=0. Likewise, oxidation by a radical (S = ½)
91 will result in one product with S=0 and one with S=½, because the unpaired electron
92 on the radical reactant pairs with one of the covalent bond electrons to produce a spin-
93 singlet.

94 Although the majority of RO₂ is formed from emitted C or H containing covalent
95 bonds, there are a few notable exceptions. Hydrogen atoms can also be produced
96 through the oxidation of CO to CO₂ by OH. During this reaction the coordinate bond

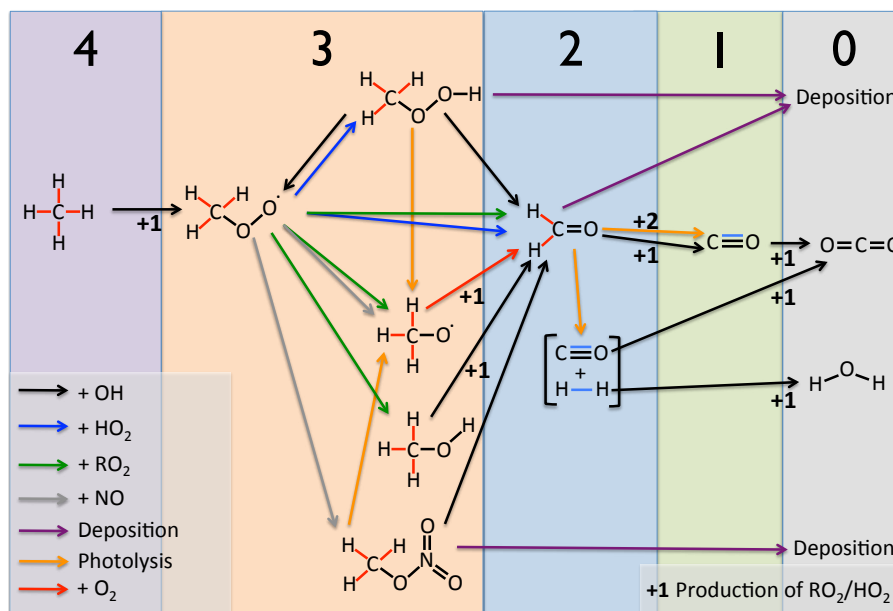


97 between the C and O atom is broken and the H atom is produced via the breaking of
98 the O-H bond. The other notable exception is the oxidation of an SO₂ lone pair of
99 electrons to SO₃ by OH, where again the H atom produced comes from the OH. In
100 both of these exceptions a spin-singlet electron pairing (CO coordinate bond or SO₂
101 lone pair) is broken during the production of the H atom, and we can therefore
102 consider these reactions as similar to the breaking of C or H containing covalent bond.
103 For simplicity these spin-singlet electron pairings that can be broken in the
104 troposphere to produce either a H atom or alkyl radical will be referred to as
105 “oxidisable bonds” (C-C, C-H, C=C, CO coordinate bond, S:).

106 Tropospheric O₃ production occurs through the oxidation of NO by RO₂. Following
107 the above rationale, these RO₂ are produced during the spin allowed breaking of
108 oxidisable bonds predominantly contained within emitted VOCs. This perspective
109 allows us to build a new metric for the production of tropospheric O₃ based around the
110 spin conserving properties of oxidisable bond breaking. In the extreme case, all
111 oxidisable bonds are photolysed to produce two spin-doublet RO₂ products, which
112 then react exclusively with NO to generate O₃. Thus at steady state, the maximum rate
113 of O₃ production is equal to the rate of production of RO₂, which is equal to twice the
114 rate of destruction of the number of oxidisable bonds. This in turn is equal to twice the
115 rate of emission of oxidisable bonds. Deviation from this maximum is determined by:

- 116 • The relative importance of processes that produce spin-singlet vs. spin-
117 doublet products during oxidisable bond breaking;
- 118 • The fraction of spin-doublet products from oxidisable bond breaking which
119 form RO₂;
- 120 • The fraction of RO₂ that go on to oxidize NO to NO₂.

121 To illustrate this Fig. 1 shows the tropospheric oxidation of a methane (CH₄) molecule
122 through various steps to either a carbon dioxide (CO₂) molecule or a species that is
123 deposited (CH₃OOH, CH₂O, CH₃NO₃). Methane contains 4 x C-H oxidisable bonds
124 (8 paired bonding-electrons) and as the oxidation proceeds, the number of oxidisable
125 bonds decays to zero. Figure 1 highlights the steps in the tropospheric CH₄ oxidation
126 mechanism that form spin-doublet products, with between 1 and 5 RO₂ produced
127 depending on the oxidation pathway. This compares with the theoretical maximum of
128 8 if all the original C-H bonds were photolysed to yield 2 spin-doublet products.



129

130 **Figure 1. Peroxy radical production during the tropospheric oxidation of CH_4 .**
 131 **Moving from left to right, the oxidisable bonds (emitted = red, produced = blue)**
 132 **present in CH_4 are removed via a range of tropospheric processes, indicated by**
 133 **the coloured arrows. The large numbers across top of the figure indicate the**
 134 **number of oxidisable bonds at each stage of this oxidation. The production of**
 135 **RO_2 is indicated by the +1/+2 numbers with the associated process arrows for**
 136 **producing 1 or 2 RO_2 respectively.**

137 The principal atmospheric source of oxidisable bonds is the emission of C-H, C-C and
 138 C=C bonds in hydrocarbons, with the only other significant sources being the
 139 emission of CO and the chemical production of CO and H_2 during hydrocarbon
 140 oxidation. Over a long enough timescale, the global atmosphere can be considered to
 141 be in a chemical steady state, where the rate of loss of oxidisable bonds is balanced by
 142 the rate of production or emission. Thus the O_3 production rate can be described by
 143 equation (1), where the O_3 production metric P_{O_3} is equal to the number of spin-
 144 paired electrons in oxidisable bonds (i.e. twice the sum of the number of oxidisable
 145 bonds emitted (E_{bonds}) and chemically produced (P_{bonds})), multiplied by the number of
 146 spin-doublet radicals produced per oxidisable bond break divided by the maximum of
 147 2 (F_{Radicals}), multiplied by the fraction of the radicals produced which are RO_2 (F_{RO_2}),
 148 multiplied by the fraction of RO_2 that goes on to react with an NO to produce an O_3



149 molecule (F_{NO}). A small correction (I) for the production of RO_2 via reactions of spin-
150 doublet radicals other than those that result in the breaking of oxidisable spin-pairings
151 (e.g. $O_3 + OH \rightarrow HO_2 + O_2$) is included.

$$152 \quad P_s O_3 = \left((2 \times (E_{bonds} + P_{bonds}) \times F_{radicals} \times F_{RO_2}) + I \right) \times F_{NO} \quad (1)$$

153 3. Implementation

154 We use the GEOS-Chem model to evaluate this new O_3 production diagnostic. GEOS-
155 Chem is a global chemical transport model of tropospheric chemistry, aerosol and
156 transport (www.geos-chem.org version 9-02). The model is forced by assimilated
157 meteorological and surface fields (GEOS-5) from NASA's Global Modelling and
158 Assimilation Office, and was run at $4^\circ \times 5^\circ$ spatial resolution. The model chemistry
159 scheme includes O_x , HO_x , NO_x , BrO_x and VOC chemistry as described in Mao et al.
160 [2013] as are the emissions. The new $P_s O_3$ diagnostic has been implemented via the
161 tracking of reactions by type in the GEOS-Chem chemical mechanism file (further
162 details given in the SI). This tracking of reactions enables the fate of all oxidisable
163 bonds as well as the production and loss of all RO_2 within the model to be determined
164 using the standard GEOS-Chem production and loss diagnostic tools. Model
165 simulations were run for 2 years (July 1st 2005 – July 1st 2007) with the first year used
166 as a spin up and the diagnostics performed on the second year.

167 The standard GEOS-Chem diagnostic for O_3 production (PO_3) is shown on the left
168 side of Table 1. This emphasizes the very fast cycling between NO and NO_2 , but
169 provides little in terms of higher process level information. The right side of Table 1
170 shows the new budget for $P_s O_3$, which tracks the processing of oxidisable bonds
171 within the model. Both diagnostic methods give the same final answer but our new
172 methodology provides more process level detail. Figure 2 illustrates this new process
173 based approach, showing the flow of emitted oxidisable spin-paired electrons (bonds)
174 to O_3 and the magnitude of the various mechanisms that contribute to and compete
175 with O_3 production. The annual oxidisable bond emission of $389 \text{ T mol yr}^{-1}$ has the
176 potential to create $778 \text{ T mol yr}^{-1}$ of radicals. If all oxidisable bonds were broken by
177 photons to produce two radical products the RO_2 production would be $778 \text{ T mol yr}^{-1}$.
178 If the oxidisable bonds were instead broken via radical reaction (e.g. OH) then RO_2
179 production would be $389 \text{ T mol yr}^{-1}$. The various oxidisable bond breaking / removal

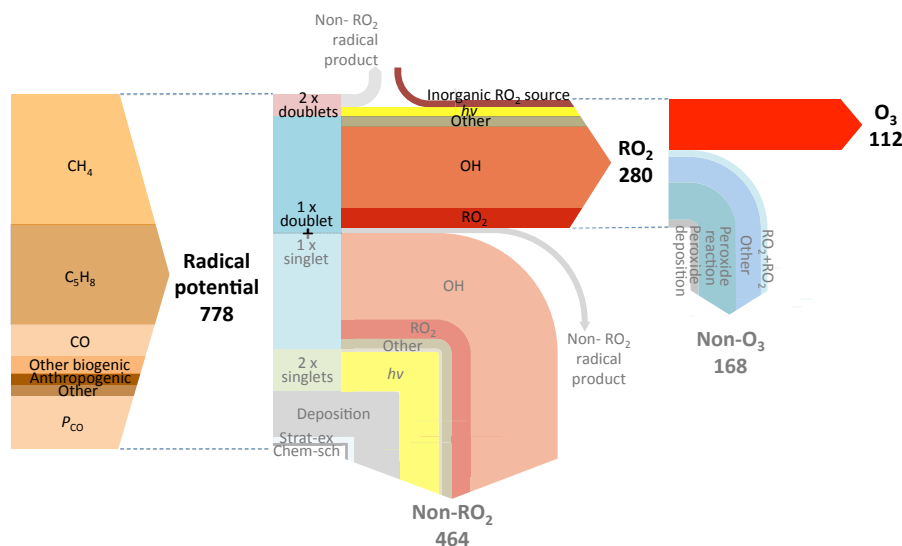


180 pathways within the model result in the production of 280 T mol yr⁻¹ of RO₂, with the
181 remainder largely producing stable spin singlet products.

182 Of the 280 T mol yr⁻¹ RO₂ produced, 112 T mol yr⁻¹ reacts with NO to produce O₃.
183 The remainder is lost through the reaction or deposition of RO₂ reservoir species
184 (RO_{2y} = RO₂ + peroxides + peroxy-acetyl nitrates). For example the production of
185 methylperoxide (CH₃O₂ + HO₂ = CH₃OOH) results in the loss of 2 RO₂'s. However,
186 the reaction of methylperoxide with OH can re-release CH₃O₂ (CH₃OOH + OH =
187 CH₃O₂ + H₂O). Thus, the production of methylperoxide represents the loss of a HO₂
188 and the movement of a CH₃O₂ into a peroxide RO_{2y} reservoir species. The deposition
189 of a peroxide molecule is thus the loss of a RO_{2y} reservoir species. Notable in Fig. 2 is
190 that the role of PAN and nitrate removal of global RO_{2y} is negligible, instead being
191 dominated by peroxide production and loss and the reaction of RO₂ with O₃.

<i>PO</i> ₃ / T mol Yr ⁻¹		<i>PO</i> ₃ / T mol Yr ⁻¹ (except <i>F</i> _{Radicals} , <i>F</i> _{RO₂} , and <i>F</i> _{NO} which are all unitless)	
NO + HO ₂ → NO ₂	74	<i>E</i> _{bonds}	330
NO + CH ₃ O ₂ → NO ₂	27	<i>P</i> _{bonds}	58
Other RO ₂ + NO → NO ₂	10	<i>F</i> _{radicals}	0.40
Other	1	<i>F</i> _{RO₂}	0.86
		Inorganic RO ₂ source	15
		<i>F</i> _{NO}	0.40
<i>PO</i>₃	112	<i>P</i>_sO₃	112

192 **Table 1. Comparison of ozone production diagnostics for GEOS-Chem base**
193 **simulation. Standard model *PO*₃ diagnostics (left column) show reactions**
194 **responsible for NO to NO₂ conversions but provide little process level**
195 **information. The new *P*_sO₃ (right) provides increased information on the**
196 **processes controlling O₃ production within the model.**



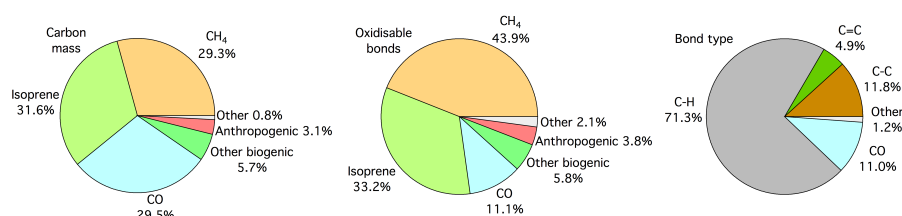
197
 198 **Figure 2. Flow of oxidisable bonds to O₃ production in the GEOS-Chem base**
 199 **simulation. Arrows are coloured according to process and the arrow thickness is**
 200 **proportional to the flux through that channel. Spin-paired electrons are input as**
 201 **oxidisable bonds into the model (left arrow), with the potential to create 778 T**
 202 **mol yr⁻¹ of radicals. The actual fate of these bonds is shown in the central arrow,**
 203 **producing 280 T mol yr⁻¹ of RO₂, of which 112 T mol yr⁻¹ reacts with NO to**
 204 **produce O₃ (right arrow).**

205 3.1 Emitted oxidisable bonds

206 The fuel for tropospheric oxidation chemistry is the emission of oxidisable bonds,
 207 predominantly in the form of hydrocarbons. The production of tropospheric O₃ from
 208 the spin-paired bonding electrons emitted into the standard GEOS-Chem model
 209 occurs with an efficiency of 14% (112 T mol yr⁻¹ molecules of O₃ produced / 778 T
 210 mol yr⁻¹ spin-paired electrons emitted as oxidisable bonds, Fig.2). These spin-paired
 211 bonding electrons are predominantly emitted in the form of CH₄, isoprene (C₅H₈) and
 212 CO (37%, 28%, and 9% respectively). Oxidisable bonds produced during chemical
 213 reactions (P_{bonds}), account for 15% of the net source. Figure 3 shows emissions of CO
 214 and hydrocarbons in the standard GEOS-Chem simulation in terms of mass of carbon
 215 per compound, number of oxidisable bonds per compound and as number of bonds in
 216 different oxidisable bond types. The commonly used carbon mass approach splits
 217 emissions approximately equally between each of the major sources (CH₄ (29%),



218 Isoprene (32%) and CO (30%). In contrast, the oxidisable bonds accounting approach
219 apportions hydrocarbon emissions 44%, 33% and 11% for CH₄, isoprene and CO
220 respectively. This highlights the high number of oxidisable bonds per carbon atom in
221 CH₄ (4) compared to isoprene (2.8) and CO (1). Thus efforts to consider emissions on
222 a per-bond basis may provide more insight into chemical processes, as it is these
223 bonds that ultimately determine the chain-like chemistry rather than the mass of
224 carbon atoms. This helps to emphasise the relative importance of CH₄ emissions on
225 global tropospheric chemistry compared with other emissions such as isoprene or CO.
226 The type of oxidisable bond emitted is overwhelmingly C-H (71%).



227
228 **Figure 3. Pie charts showing hydrocarbon emissions in the base GEOS-Chem**
229 **simulation. Emissions split by carbon mass (left), number of oxidisable bonds**
230 **(centre) and bond type (right).**

231 The total emission and production of oxidisable bonds has the potential to create 778
232 T mol yr⁻¹ of radicals. However, only 6% of the oxidisable spin-pairings are broken to
233 give the maximum 2 spin-doublet products (e.g. radical channel of CH₂O photolysis).
234 The majority (68%) are oxidized via reaction with a spin-doublet species (OH) to
235 produce 1 spin-singlet and 1 spin-doublet product (e.g. OH + VOC). The remaining
236 26% of spin-paired electrons are removed to form two spin-singlets (e.g. the non-
237 radical channel of CH₂O photolysis). Thus, of the 778 Tmol yr⁻¹ spin-paired electrons
238 emitted or produced only 265 T mol yr⁻¹ (34%) are converted into RO₂, with an
239 additional 15 T mol yr⁻¹ produced from reactions such as O₃ + OH → HO₂ + O₂ (*I*).
240 The efficiency of O₃ production from the available oxidisable bonds is further reduced
241 as only 40% of the 280 T mol yr⁻¹ of RO₂ produced react with NO to produce NO₂.
242 The remainder is lost either through the self-reaction of RO₂ or via loss through
243 deposition or reaction of RO_{2y} reservoir species (e.g. peroxides). Thus overall 14% of
244 the emitted bonding electrons go on to make O₃.

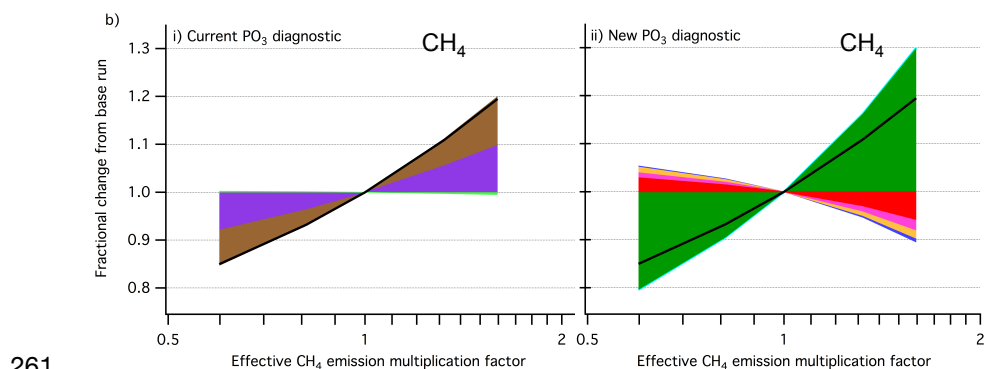
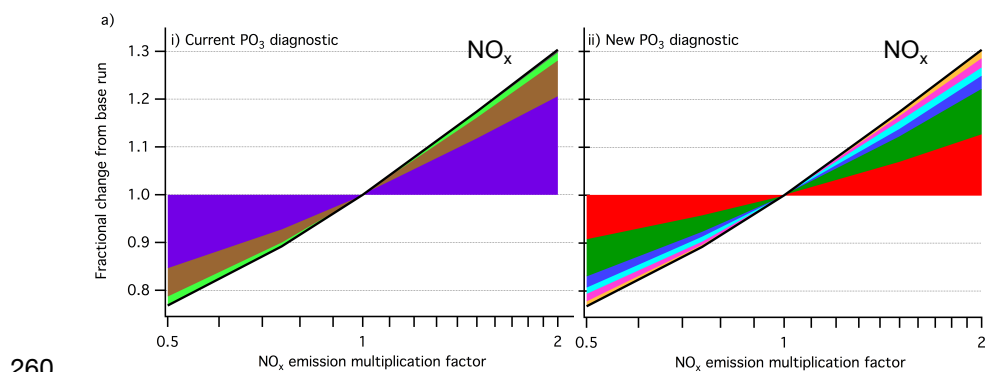
245 This new O₃ production diagnostic shows the impact of processes such as emission,
246 deposition and chemical mechanism, providing significantly more detail than the

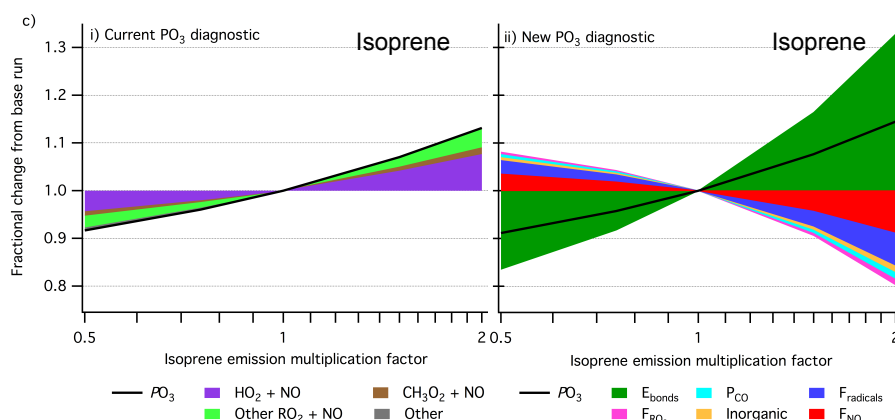


247 standard PO_3 diagnostic approach (Table 1). We now explore the sensitivity of model
248 O_3 production to changing emissions of NO_x and VOC from the perspective of the
249 two diagnostic methods.

250 4 Model sensitivities

251 Understanding model response to changing emissions is an important tool for
252 considering policy interventions. The major controls on O_3 production are emissions
253 of NO_x and VOCs. We show in Fig. 2 that from the perspective of global O_3
254 production, oxidisable bond emissions are dominated by CH_4 and isoprene. Figure 4
255 shows the impact of changing emissions of NO_x , isoprene and CH_4 on O_3 production
256 from both the perspective of this new methodology and the conventional $NO+RO_2$
257 diagnostic approach. The following sections investigate these model responses and
258 use the new diagnostic to provide insight into the processes driving the observed
259 response in O_3 production.





262
 263 **Figure 4. Understanding the effect of NO_x and VOC emissions on ozone**
 264 **production at the process level. Stack plots showing fractional change in model**
 265 **PO₃ compared to base simulation and associated contributions from the current**
 266 **PO₃ (i) and new P_sO₃ (ii) diagnostic parameters under changing NO_x emissions**
 267 **(a), effective CH₄ emission (b) and isoprene emission (c).**

268 4.1 NO_x emissions

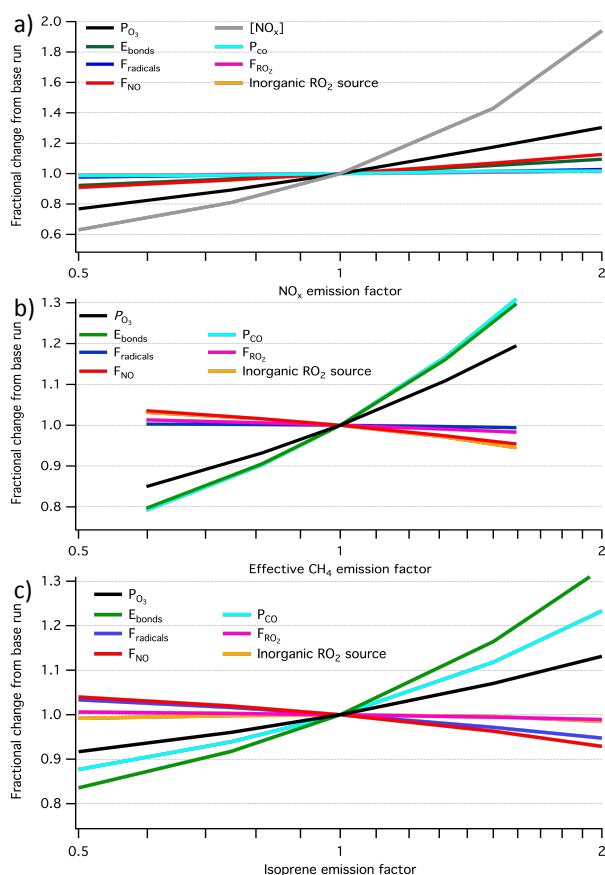
269 Figure 4a diagnoses the relative response of GEOS-Chem O₃ production to changing
 270 NO_x emissions, using simulations where NO_x emissions from anthropogenic, biomass
 271 burning, biofuels, soil and lighting sources were multiplied by factors of 0.5 - 2.
 272 Increasing NO_x emissions increases O₃ production. The standard RO₂+NO diagnostic
 273 (Fig.4a(i)) shows that fractional contributions to the total change in PO₃ from HO₂
 274 (67%), methyl-peroxy (MO₂) (25%), and other RO₂ (8%) remain approximately
 275 constant across the NO_x emission range investigated. This diagnostic provides little
 276 detail on the processes driving the change in O₃ production under changing NO_x
 277 emissions. In contrast, Fig. 4a(ii) is based on the new P_sO₃ diagnostic and shows a
 278 range of process level changes occurring as NO_x emissions change.

279 4.1.1 Impact of changing NO_x emission on F_{NO}

280 Unsurprisingly, as NO_x emissions increase the fraction of RO₂ reacting with NO to
 281 produce NO₂ (F_{NO}) increases (red section in Fig. 4a(ii)). However, this impact only
 282 accounts for around 40% of the increase in P_sO₃. Figure 5a shows the fractional
 283 change in all the P_sO₃ efficiency parameters and the global mean NO_x concentration
 284 as a function of the changing NO_x emission. As NO_x emissions increase the increase



285 in NO_x concentration in the model is somewhat dampened. Halving the NO_x emission
 286 leads to NO_x burdens dropping by $\sim 35\%$, and doubling leads to an increase of 95%.
 287 This dampening is due to the impact of NO_x emissions on OH (see section 4.1.2),
 288 which is the dominant sink for NO_x . Increasing NO_x increases OH concentrations,
 289 which in turn shortens the NO_x lifetime thus dampening the response of concentration
 290 to emission.



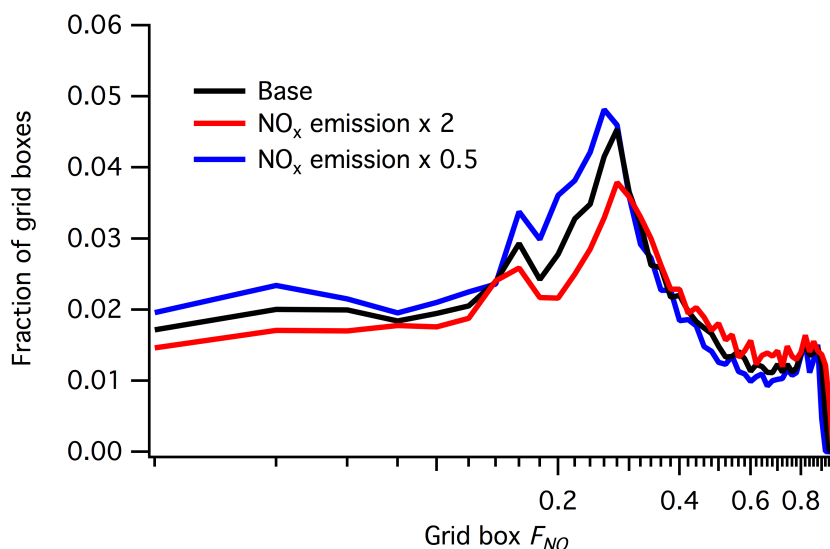
291

292 **Figure 5. Fractional change in new P_{O_3} diagnostic parameters from base run**
 293 **against changing NO_x emission (a); effective CH_4 emission (b); and isoprene**
 294 **emission (c).**

295 The response of F_{NO} to changes in NO_x emissions is also dampened relative to the
 296 change in NO_x emissions. This is due to spatial variability in F_{NO} , which is not
 297 affected uniformly by changing NO_x emissions. Figure 6 shows the probability



298 distribution of F_{NO} values across all model grid boxes for the base simulation and the
299 half and doubled NO_x emission simulations (black, blue and red lines respectively).
300 For example, in a grid-box in the continental boundary layer where RO_2 reacts
301 overwhelmingly with NO , doubling the NO_x emission may move F_{NO} from 0.90 to
302 0.95 but it can't double it. Similarly, in the remote boundary layer where RO_2 reacts
303 overwhelmingly with other RO_2 doubling NO_x emissions may move F_{NO} from 0.3 to
304 0.4 but again it doesn't double. Thus the geographical spread of NO_x chemistry limits
305 the change in F_{NO} caused by changing NO_x emissions. The spatial variability in the
306 new P_sO_3 diagnostic parameters shows that this approach has significant potential in
307 the analysis of regional O_3 budgets as well as global.



308

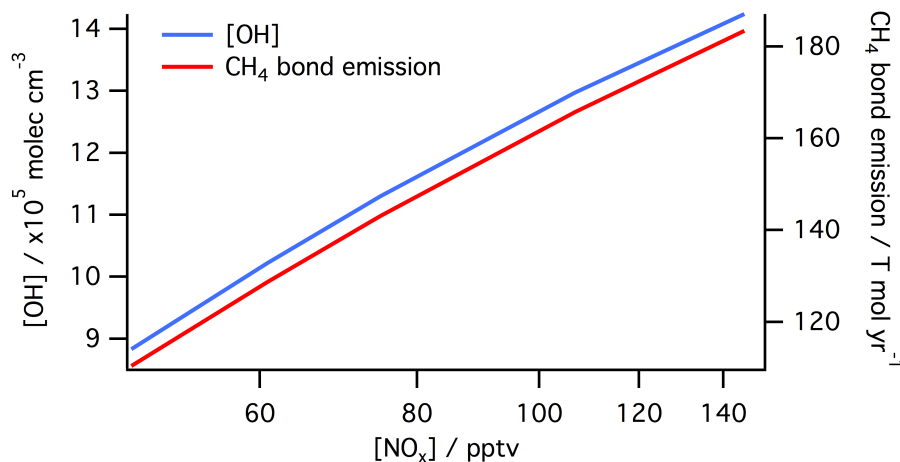
309 **Figure 6. Effect of NO_x emission on distribution of F_{NO} values (log scale). F_{NO}**
310 **values for each model grid box in the base and NO_x emission x 0.5 and x 2**
311 **simulations, split into 50 x 0.02 width bins.**

312 4.1.2 Impact of changing NO_x emission on E_{bonds}

313 Figure 4a(ii) shows that 60% of the response in P_sO_3 to changing NO_x emission is due
314 to factors other than F_{NO} , with 40% of the increase due to changes in the emissions
315 (E_{bonds} : 32%) and chemical production (P_{bonds} : 8%) of oxidizable bonds. This increase
316 in E_{bonds} is surprising given VOC emissions are unchanged in these simulations.
317 However, increasing NO_x emissions results in an increased OH concentration in the



318 model, which then leads to an increase in CH₄ oxidation. GEOS-Chem fixes CH₄
319 concentrations resulting in an increase in the effective CH₄ emissions as OH
320 concentrations increase, causing an increase in the total bond emission (E_{bonds}). Figure
321 7 shows the response of model global mean OH concentration and effective CH₄ bond
322 emission as a function of global mean NO_x concentration across the simulations where
323 the base NO_x emissions are multiplied by factors from 0.5 to 2. More CH₄ oxidation
324 also leads to more CH₂O production and in turn more CO production (P_{CO}),
325 accounting for a significant fraction of the increase in this term.



326

327 **Figure 7. Global mean OH concentration and effective CH₄ emission as a**
328 **function of [NO_x]. Plot shows effective CH₄ emission tracks OH concentration in**
329 **simulations where the NO_x emission was increased or decreased from the base**
330 **simulation. Note X-axis log scale.**

331 4.1.3 Impact of changing NO_x emission on F_{radicals} , F_{RO_2} and I

332 The fraction of radicals produced from bond oxidation (F_{radicals}) and the fraction of
333 those radicals which are RO₂ (F_{RO_2}) show slight positive increase with NO_x emission,
334 accounting for 9% and 6% of the change in $P_s\text{O}_3$ respectively. This reflects changes in
335 the partitioning of the fate of the oxidisable bonds, and is largely due to the changes in
336 OH. As OH increases with NO_x emission, the rate of chemical oxidation of bonds
337 increases at the expense of other losses, in particular deposition. The inorganic RO₂
338 source term (I) also correlates with NO_x emission, as it is largely determined by the



339 concentrations of OH and O₃. This change accounts for 5% of the observed change in
340 P_sO_3 .

341 Thus, with this new diagnostic methodology it is evident that only 40% of the model
342 O₃ production response to changing NO_x emission is due to the direct effect of
343 increasing NO concentration on the rate of RO₂ + NO reactions. Another 40% is due
344 to fixing the concentration of CH₄ within the model, with the final 20% due to the
345 increased OH competing for the available oxidisable bonds.

346 4.2 Changing effective CH₄ emissions

347 Figure 4b shows the effect on the O₃ production diagnostic of varying the prescribed
348 CH₄ concentrations by factors of between 0.5 and 2 from the base simulation. The
349 CH₄ emission rate (plotted) is diagnosed from the loss rate of CH₄ to reaction with
350 OH, the only CH₄ loss in the model. We describe this as the effective CH₄ emission.

351 As effective CH₄ emission increases, O₃ production also increases. The standard
352 diagnostic (Fig.4b(i)) shows that this increase occurs through an increased rate of
353 reaction of HO₂ and CH₃O₂ with NO, as would be expected as these are the RO₂
354 produced during CH₄ oxidation. The rate of other RO₂ + NO reactions actually
355 decreases slightly as CH₄ emissions increase, due to lower OH concentrations and
356 increased competition for NO from HO₂ and CH₃O₂. The new diagnostic (Fig.4b(ii)),
357 however, shows the increase in O₃ production with increasing effective CH₄ emission
358 is not simply a result of more HO₂ and MO₂.

359 4.2.1 Impact of changing effective CH₄ emission on F_{NO}

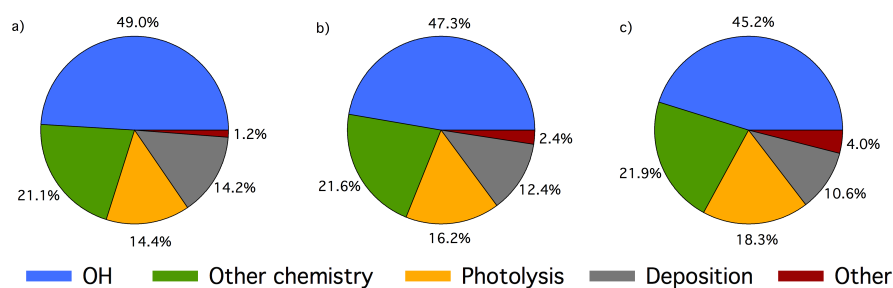
360 The observed change in P_sO_3 is around one third smaller than would be expected from
361 the increase in the oxidisable bond emission (E_{bonds}) and bond production (P_{bonds})
362 terms alone. This is due to a countering decrease in the other efficiency parameters
363 with increasing effective CH₄ emission. Figure 5b shows the fractional change in all
364 the efficiency parameters as a function of the changing effective CH₄ emission. The
365 decrease in the fraction of RO₂ reacting with NO to produce NO₂ (F_{NO}) is driven by
366 increasing O₃ concentrations, which push the NO/NO₂ ratio towards NO₂. This
367 reduces the availability of NO to react with RO₂ thereby reducing O₃ production. This
368 shift in the NO/NO₂ ratio also increases NO_x loss within the model with increasing
369 CH₄ emission, as the increased CH₄ oxidation increases RO₂ concentrations resulting



370 in larger losses of NO₂ via compounds such as peroxyacetyl nitrate (PAN) and
371 peroxyntitric acid (PNA).

372 4.2.2 Impact of changing effective CH₄ emission on E_{bonds}

373 As CH₄ is the largest single source of oxidisable bonds (Fig. 3), increasing the
374 effective CH₄ emission results in an increase in E_{bonds}. Changing the fraction of total
375 emitted oxidisable bonds from CH₄ does however have significant consequences on
376 the loss mechanisms of these bonds, which influences the other efficiency parameters.
377 The pie charts in Fig. 8 show the split of oxidisable bond loss mechanisms in the base
378 simulation and those with the CH₄ concentration fields multiplied by 0.5 and 2. As the
379 effective CH₄ emission increases the fraction of bonds lost via OH decreases, despite
380 the actual number of oxidisable bonds lost to OH increasing. A larger fraction of
381 bonds are therefore lost via the other mechanisms shown in Fig. 8 rather than reaction
382 with OH. As CH₄ removal occurs predominantly in the free troposphere, increasing
383 the effective CH₄ emission also results in a reduction in the fraction of oxidisable
384 bonds lost via deposition. The largest fractional increase in bond loss mechanism with
385 increasing effective CH₄ emission is for photolysis, with the increase in the “other”
386 fraction due to increased loss of bonds to the stratosphere with increasing CH₄. The
387 fraction of bonds lost via other chemistry (e.g. non-OH radical oxidation and RO₂ self
388 reactions) remains approximately constant across the effective CH₄ emission scenarios
389 investigated.



390
391 **Figure 8. Oxidisable bond loss mechanisms under changing CH₄ emissions. Pie**
392 **charts showing fractional loss mechanisms for oxidisable bonds in model**
393 **simulations with 0.5 x CH₄ concentration field (a), base simulation (b) and 2 x**
394 **CH₄ concentration field.**



395 4.2.3 Impact of changing effective CH₄ emission on F_{radicals} , F_{RO_2} and I

396 The fraction of oxidisable bonds that goes on to produce radicals (F_{radicals}) and the
397 fraction of these that are RO₂ (F_{RO_2}) also decrease with increasing effective CH₄
398 emissions. This is due to decreasing global OH concentration resulting from increased
399 loss by reaction with CH₄ and a decreasing NO concentration. This favours bond loss
400 via pathways such as deposition rather than those that produce RO₂. These changes
401 are predominantly due to the chemistry of CH₂O. As shown in Fig. 1, the oxidation of
402 CH₂O occurs either via reaction with OH or photolysis, with OH reaction yielding 1
403 RO₂ from the net breaking of 2 spin-singlet bonds, and the two photolysis channels
404 yielding either 0 x RO₂ (spin-singlet products molecular channel) or 2 x RO₂ (spin-
405 doublet products radical channel), with the molecular channel being dominant. The
406 reduction in OH concentration with increasing CH₄ means photolysis increases its
407 competition as a bond loss mechanism, which has the effect of reducing the average
408 RO₂ production per CH₂O oxidised. The increase in the fraction of total bonds lost
409 through the CH₂O photolysis as CH₄ increases thus results in a reduction in both
410 F_{radicals} and F_{RO_2} . The reduction in F_{radicals} due to changing CH₂O fate, however, is
411 largely offset by a reduction in the fraction of bonds lost via deposition as CH₄
412 increases. This is due to the long lifetime of CH₄ compared with the majority of other
413 sources of oxidisable bonds, resulting in oxidation increasing fractionally in the free
414 troposphere where deposition is a less significant loss mechanism than in the
415 boundary layer.

416 4.3 Changing isoprene emission

417 The species through which the oxidisable bonds are emitted has a significant impact
418 on O₃ production, due to their subsequent removal mechanisms. For example, in a
419 simulation where the only emission of oxidisable bonds is CO, F_{radicals} is 0.5 and F_{RO_2}
420 is 1 as the only CO sink is reaction with OH to produce one HO₂ (OH + CO → HO₂ +
421 CO₂). The CO coordinate bond, which in theory has the potential to produce 2
422 radicals, only produces 1 radical, which is an RO₂.

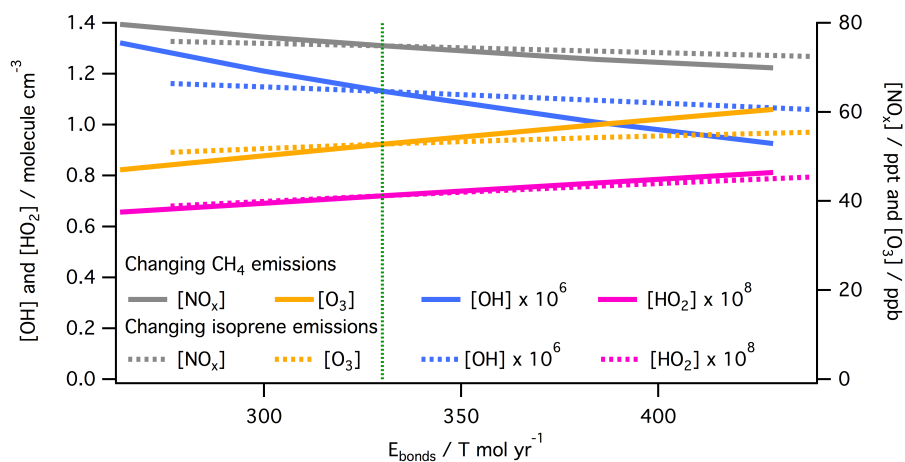
423 Isoprene has the most complex chemistry in the model and is the second largest
424 source of bonds into the atmosphere (Fig. 3). Figure 4c shows the response of the two
425 O₃ production diagnostics to varying the isoprene emission within the model. The
426 standard diagnostic (Fig.4c(i)) shows that the most significant increase in PO_3 from



427 increasing isoprene emissions is from $\text{NO} + \text{HO}_2$ and non- MO_2 peroxy radicals, with a
428 smaller increase from MO_2 . The new $P_5\text{O}_3$ diagnostic (Fig.4c(ii)) again provides more
429 insight, showing significant offsetting of around a half between the terms.

430 4.3.1 Impact of changing isoprene emission on F_{NO}

431 The increased isoprene emission leads to a similar change in the magnitude of the
432 total number of oxidisable bonds emitted (E_{bonds}) as the simulations in which effective
433 CH_4 emission were varied. However, the countering decrease in all of the efficiency
434 parameters is much larger for isoprene than for CH_4 . Figure 5c shows the fractional
435 change in the new $P_5\text{O}_3$ ozone production diagnostic parameters as a function of
436 isoprene emissions compared to the base simulation. The change in F_{NO} is due to both
437 a decrease in global mean NO_x concentrations with increasing isoprene and the spatial
438 distribution of isoprene emissions. With the majority of global isoprene emissions
439 being in regions with low NO_x emissions, and thus low values of F_{NO} . Figure 9 shows
440 a decrease in global mean NO_x , and global mean OH, concentrations with increasing
441 isoprene emissions, however, the effect is less than that seen when CH_4 is responsible
442 for the same increase in oxidisable bond emission. This is due in a large part to the
443 spatial scales over which the two compounds impact.



444

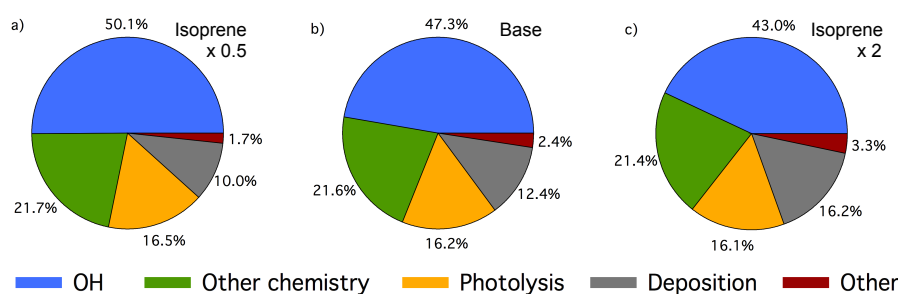
445 **Figure 9.** The effect of oxidisable bond parent species on OH, HO_2 , O_3 and NO_x
446 concentrations. Global mean [OH], [HO_2], [O_3] and [NO_x] for simulations where
447 the effective CH_4 emission (solid lines) and isoprene emission (dashed lines) were
448 changed, against model E_{bonds} . The dashed vertical green line indicates E_{bonds} in
449 the base simulation ($330 \text{ T mol yr}^{-1}$).



450 4.2.2 Impact of changing isoprene emission on E_{bonds}

451 As isoprene is the second largest source of oxidisable bonds (Fig. 3), increasing the
452 isoprene emission results in a significant increase in E_{bonds} . Differences in both the
453 spatial distribution of emissions and the oxidation chemistry of isoprene and CH_4 ,
454 however, means that the impact of the increases in E_{bonds} on O_3 production are
455 significantly different for the two compounds. This is predominantly because the
456 fraction of oxidisable bonds that are physically deposited for isoprene is high
457 compared to those emitted as CH_4 . This increase is due to i) the higher solubility of
458 isoprene oxidation products compared to those of CH_4 , and ii) the higher reactivity of
459 isoprene means its oxidation occurs in the boundary layer where both dry and wet
460 deposition is most effective.

461 Figure 10 shows the split of oxidisable bond loss mechanisms in the base simulation
462 and those with the isoprene emissions multiplied by 0.5 and 2. The complex myriad of
463 products formed during the isoprene oxidation mechanism also results in the
464 production of many highly oxygenated multifunctional compounds with high Henry's
465 law solubility constants, meaning they are more readily lost to deposition.



466 OH Other chemistry Photolysis Deposition Other
467 **Figure 10. Oxidisable bond loss mechanisms under changing isoprene emissions.**
468 **Pie charts showing fractional loss mechanisms for oxidisable bonds in model**
469 **simulations with 0.5 x isoprene emission (a), base simulation (b) and 2 x isoprene**
470 **emission (c).**

471 Increasing the isoprene emission also has a slight offsetting impact on the effective
472 CH_4 emission, as increased isoprene concentrations decrease OH concentrations, and
473 thus decrease the effective CH_4 emission. A doubling in isoprene emission causes a
474 6% reduction in the effective emission of CH_4 .

475



476 **4.3.3 Impact of changing isoprene emission on F_{radicals} , F_{RO2} and I**

477 As shown in Fig. 3c(ii), increasing the isoprene emission results in a reduction in all
478 P_sO_3 efficiency parameters. The reductions in F_{radicals} is due to the higher fraction of
479 oxidisable bonds that are lost via non-radical forming pathways (e.g. deposition) for
480 isoprene relative to the other main oxidisable bond emission sources CH_4 and CO .
481 The slight decreases of F_{RO2} and I with increasing isoprene emission are
482 predominantly due to changes in OH and NO_x (Fig. 9).

483 The complex chemistry of isoprene oxidation combined with the spatial distribution of
484 isoprene emissions means the increase in O_3 production due to increases in isoprene
485 emissions is roughly half what might be expected from the increase in oxidisable bond
486 emission alone (i.e. if the increase was *via* CO instead of isoprene).

487 **5. Conclusions**

488 We have shown that this bond-focussed approach to O_3 production provides a
489 significantly more detailed understanding of the processes involved. The role of
490 modelled VOC emissions and O_3 burden has been reported previously [*Wild, 2007*;
491 *Young et al., 2013*]. However previous efforts extending this to a general process led
492 approach has not been successful. This new approach provides a tool with which the
493 processes controlling O_3 production can be investigated, and a metric by which
494 different emissions can be compared. For example, the differing chemistry of isoprene
495 and CH_4 shows that even though their emissions of carbon mass are comparable, the
496 atmosphere responds in different ways, with the isoprene bonds being less effective in
497 producing O_3 than CH_4 bonds. By quantifying multiple steps in the O_3 production
498 process, competing changes in the system become apparent (as shown in Fig. 4b(ii)
499 and c(ii)) and are thus testable. This enables the effect of model approximations on O_3
500 production to be quantified (e.g. the effect of NO_x on CH_4 emissions when using CH_4
501 concentration fields).

502 This new diagnostic also points towards the importance of observational datasets for
503 assessing our understanding of tropospheric chemistry. Although the budget presented
504 in Fig. 2 provides an annually integrated global estimate it points towards local
505 comparisons that can be made to assess model fidelity. Comparisons, both their
506 magnitude and their ratios, between observed and modelled bond concentration, bond
507 emission and loss fluxes (e.g. OH reactivity [*Yang et al., 2016*] or depositional fluxes



508 [*Wesely and Hicks, 2000*]), and O₃ production [*Cazorla and Brune, 2010*] would all
509 provide comparisons for outputs from the *P_sO₃* diagnostic and help assess model
510 performance.

511 Another potentially important application is in model-model comparisons. Increases
512 in our understanding of why different models calculate different O₃ production and
513 burdens has been slow [*Stevenson et al., 2006; Wu et al., 2007; Young et al., 2013*]. A
514 comparison between models based on this methodology may well help identify at a
515 process level why models differ in their O₃ production. The application of this
516 diagnostic to regional O₃ production should also increase insight into the processes
517 controlling model O₃.

518 **References**

- 519 Cazorla, M., and W. H. Brune (2010), Measurement of ozone production sensor,
520 *Atmos. Meas. Tech.*, 3(3), 545–555, doi:10.5194/amt-3-545-2010.
- 521 Crutzen, P. J. (1971), Ozone production rates in an oxygen-hydrogen-nitrogen oxide
522 atmosphere, *J. Geophys. Res.*, 76(30), 7311–7327,
523 doi:10.1029/JC076i030p07311.
- 524 Kroll, J. H. et al. (2011), Carbon oxidation state as a metric for describing the
525 chemistry of atmospheric organic aerosol., *Nat. Chem.*, 3(2), 133–139,
526 doi:10.1038/nchem.948.
- 527 Larson, R. A., and K. A. Marley (1999), Singlet oxygen in the environment, *Environ.*
528 *Photochem.*, 2, 123–136.
- 529 Levy, H. (1973), Photochemistry of minor constituents in the troposphere, *Planet.*
530 *Space Sci.*, 21(4), 575–591, doi:10.1016/0032-0633(73)90071-8.
- 531 Mao, J., F. Paulot, D. J. Jacob, R. C. Cohen, J. D. Crouse, P. O. Wennberg, C. A.
532 Keller, R. C. Hudman, M. P. Barkley, and L. W. Horowitz (2013), Ozone and
533 organic nitrates over the eastern United States: Sensitivity to isoprene chemistry,
534 *J. Geophys. Res. Atmos.*, 118(19), 1–13, doi:10.1002/jgrd.50817.
- 535 Nguyen, M. T., R. Sumathi, D. Sengupta, and J. Peeters (1998), Theoretical analysis
536 of reactions related to the HNO₂ energy surface: OH + NO and H + NO₂, *Chem.*
537 *Phys.*, 230(1), 1–11, doi:10.1016/S0301-0104(97)00383-2.
- 538 Stevenson, D. S. et al. (2006), Multimodel ensemble simulations of present-day and
539 near-future tropospheric ozone, *J. Geophys. Res. Atmos.*, 111(8),
540 doi:10.1029/2005JD006338.
- 541 Wesely, M. L., and B. B. Hicks (2000), A review of the current status of knowledge
542 on dry deposition, , 34.
- 543 Wild, O. (2007), Modelling the global tropospheric ozone budget: exploring the
544 variability in current models, *Atmos. Chem. Phys.*, 7, 2643–2660,
545 doi:10.5194/acpd-7-1995-2007.
- 546 Wu, S., L. J. Mickley, D. J. Jacob, J. A. Logan, R. M. Yantosca, and D. Rind (2007),
547 Why are there large differences between models in global budgets of



548 tropospheric ozone?, *J. Geophys. Res. Atmos.*, *112*(5), 1–18,
549 doi:10.1029/2006JD007801.

550 Yang, Y., M. Shao, X. Wang, A. C. Nölscher, S. Kessel, A. Guenther, and J. Williams
551 (2016), Towards a quantitative understanding of total OH reactivity: A review,
552 *Atmos. Environ.*, *134*(2), doi:10.1016/j.atmosenv.2016.03.010.

553 Young, P. J. et al. (2013), Pre-industrial to end 21st century projections of
554 tropospheric ozone from the Atmospheric Chemistry and Climate Model
555 Biogeosciences Intercomparison Project (ACCMIP), *Atmos. Chem. Phys.*,
556 *13*(10), 5277–5298, doi:10.5194/acp-13-5277-2013.

557

558 **Author contributions**

559 All work presented here was conceived by P.M.E. and M.J.E. The implementation,
560 model simulations and analysis were carried out by P.M.E., and the manuscript was
561 written by P.M.E. with substantial input from M.J.E..

562 **Additional information**

563 The authors declare no competing financial interests.

564 **Acknowledgements**

565 P.M.E. was supported by NERC Grant NE/K004603/1. This work was also supported
566 by the NERC funded BACCHUS project (NE/L01291X/1). GEOS-Chem
567 (www.geos-chem.org) is a community effort and we wish to thank all involved in the
568 development of the model.